Design guidelines for edge-coupled waveguide unitraveling carrier photodiodes with improved bandwidth

Pedram Razavi [1], Stefan Schulz [1*], Brendan Roycroft[1], Brian Corbett[1], Eoin P. O'Reilly[1,2]

[1] Tyndall National Institute, University College Cork, Lee Maltings, Dyke Parade, T12 R5CP Cork, Ireland
[2] Department of Physics, University College Cork, T12 YN60 Cork, Ireland
[*] stefan.schulz@tyndall.ie

Abstract: This paper presents experimental and simulation results for edge-coupled waveguide unitraveling-carrier photodiodes based on an InGaAs/InP heterostructure. Experimental results are used to calibrate the numerical device simulator. We study how different aspects of the unitraveling-carrier photodiode epistructure and contacts impact on the overall device bandwidth, calculating the photoresponse for different structural parameters and doping concentration profiles. The effect of these parameters on the 3-dB cut-off frequency is studied, and design guidelines for unitraveling-carrier photodiodes with improved performance are presented. The unitraveling-carrier photodiode simulated using our design guidelines has a 3dB cut-off frequency of 49 GHz, a factor of two larger than the 25 GHz cut-off of the fabricated UTC photodiode.

1. Introduction

Photodiodes (PDs) are used to convert optical signals into electric signals with several applications in optical communication and measurement systems [1], such as camera light meters. Large 3-dB bandwidth, high photocurrent and high responsivity are very important features of PDs for developing high capacity optical communication and fast measurement systems [2], [3]. The unitraveling-carrier photodiode (UTC PD) is a relatively new type of PD whose main attraction is its capability for high bandwidth and high current operation [4]. These PDs, in which electrons are the only active carriers, have reduced space charge saturation effects when compared with traditional PIN PDs, thanks to their different operation mechanism and the higher drift velocity of electrons than holes [5]. Band profiles of UTC and PIN PD structures are shown in Figure 1 (a) and (b), respectively. UTC PDs contain a narrow-gap p-type light absorption layer and a wide-gap undoped/lightly doped depleted carrier collection layer [6]. The light absorption in the p-doped absorption region generates the electron-hole pairs. The electrons generated in this region, which are the minority carriers, will be blocked from diffusing towards the anode side by a diffusion barrier layer. Therefore, electrons move towards the collection layer. The very small energy relaxation of the majority hole carriers in the absorption region makes the response times of the photo-generated holes negligible [7], [8]. Therefore only generated electrons are considered as active carriers. Because of the much higher electron drift velocity compared to that of the holes, space charge saturation effects are reduced and a higher speed and output can be achieved [4], [6] when compared to a traditional PIN PD.

Different techniques can be found in the literature for improving the performance of UTC-PDs [9]. These include adding an undoped layer (depleted absorber) between the absorption layer and the collection layer [10] to increase responsivity and facilitate electron transit. Furthermore, the performance can be further enhanced by adding a cliff layer [11], [12] to tailor the electric field and thus to improve electron transit, using a dual-drifting layer [13] which consists of a velocity overshoot and a velocity saturation layer.

Here, in this paper, our goal is to increase the 3-dB cut-off frequency (f_{3dB}) of UTC PDs for faster optical communications while understanding the underlying reasons for this increase. To do so, we consider some of the main techniques for improving the performance of UTC PDs, investigating the effect of different structural parameters on f_{3dB} for an edge-coupled waveguide (WG) InGaAs/InP heterostructure UTC-PD. The edge-coupled geometry is chosen as it can have higher responsivity due to the longer length of the absorption region when compared with a surface normal geometry. The UTC PD investigated utilizes depleted absorber and cliff layers to improve electron transit. Based on the analysis presented, we introduce design guidelines to optimize UTC PDs and enhance the 3-dB cut-off frequency. Our findings show that the structure of the edge-coupled WG UTC PDs considered here has a significant impact on the bandwidth limits. The paper is structured as follows. In Section 2 device fabrication is briefly explained. Section 3 discusses the methods and theoretical models which were used, while Section 4 contains experimental results and model calibration. In Section 5 we present simulation results and discussions, and finally we conclude in Section 6.

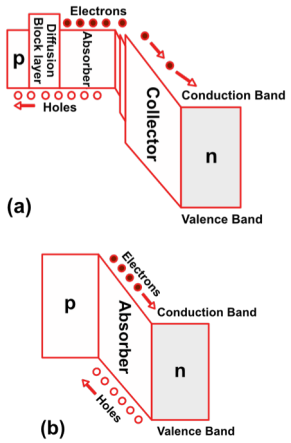

Fig. 1. *Energy band profiles for* ***(a)*** *a UTC photodiode and* ***(b)*** *a PIN photodiode.*

2. Device fabrication

Metalorganic vapour phase epitaxy is used to grow the UTC-PDs. The grown structure is described in Table 1 (specifying all structural parameters), and the fabricated photodiode is shown in Fig. 2. PDs are fabricated based on structures previously presented in the literature [4], [14]. A schematic 2D illustration of the edge-coupled WG UTC-PD, which has been used in this work, is depicted in Fig. 3. Note that the n-contact surface is much wider than the p-contact, as can be seen in Fig. 2. We have used Zn and Si for p and n doping, respectively. We also include barrier-reduction layers to help the carriers flow across heterojunctions. Electrical measurements of the devices have been performed and C-V profiles are used to analyze the DC characteristics. The ridge width is 5.5 µm and the ridge lengths are 25 µm and 65 µm, respectively.

3. Methods and theoretical models

We use the commercial Silvaco ATLAS software [15] to investigate the RF response of the device. The simulation parameters are set according to the simulation software user's manual. The theoretical models have been calibrated by modifying parameters such as contact resistance and using the proper physical models to reproduce the experimental results, as discussed below. The p-contact resistance is set for the PD ridge width and length of 5.5 µm and 25/65 µm, respectively. The n-contact resistance is set to be 5 times smaller than the p-contact resistance, reflecting the wider n-contact of our grown UTC-PD. We use the Fermi-Dirac carrier statistics model together with the drift-diffusion (DD) method for carrier transport. We also employ the energy balance model which uses a higher order approximation of the Boltzmann transport equation to account for non-local effects (such as velocity overshoot) [15]. Moreover, in low field mobility we use concentration dependent mobility models (ANALYTIC and CONMOB) in which the mobility is related to the doping density. For velocity saturation in high electric field, we employ a field dependent mobility model (FLDMOB), which takes into account the lateral electric field dependence in the direction of the current flow [16]. To model non-radiative carrier recombination, Shockley-Read-Hall (SRH), concentration-dependent SRH (CONSRH), and Auger recombination models have been chosen [15]. Numerical solutions are obtained using the Newton method. The composition of the InGaAsP barrier reduction layer is chosen as $In_{0.713}Ga_{0.287}As_{0.62}P_{0.38}$ to be lattice-matched with InP and at the same time to provide an optimum charge transfer across heterojunctions.

4. Experimental results and model calibration

To study experimentally the properties of the above discussed UTC PD, side illumination at 1.55-µm wavelength with a power density of $1x10^4$ W/cm^2 is used. A lens ended fibre is used to couple light into the waveguide. In Figure 4, the measured RF response for the 5.5 µm x 25 µm long device is shown for different bias voltages down to -10 V. Here, the device was probed using an Anritsu 65 GHz vector network analyser (VNA) and a Cascade Microtech 67 GHz GSG probe. The VNA was calibrated to the probe tips using a SOLT calibration chip. The optical modulation was

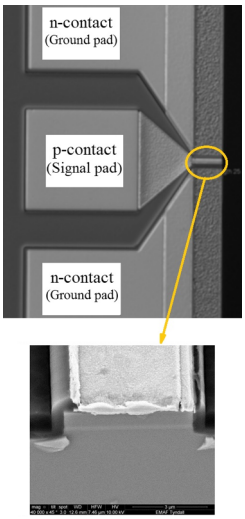

Fig. 2. *Optical microscope image of the ridged UTC-photodiode.*

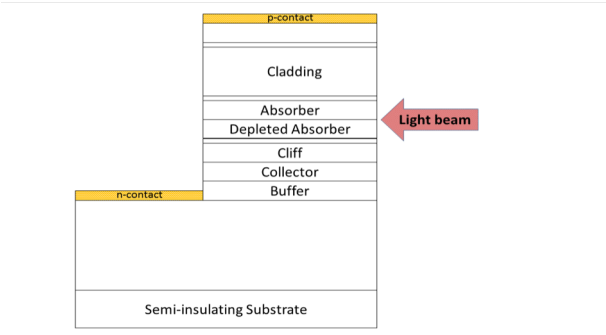

Fig. 3. *Schematic 2D illustration of the initially fabricated UTC photodiode.*

Table 1 Structural parameters of the epistructure used in the initial UTC photodiode.

Material	Thickness (nm)	Type	Doping (cm^{-3})
InGaAs (contact+)	60	p	>3 × 10^{19}
InGaAs (contact)	40	p	1 × 10^{19}
InGaAsP (barrier reduction)	20	p	2 × 10^{18}
InP (cladding)	600	p	2 × 10^{18}
InGaAsP (barrier reduction)	20	p	2 × 10^{18}
InGaAs (absorber)	50	p	1 ×10^{19}
InGaAs (depleted absorber)	50	n	1-2 × 10^{16}
InGaAsP (barrier reduction)	20	n	2 × 10^{16}
InP (cliff)	50	n	2 × 10^{17}
InP (collector)	50	n	2 × 10^{16}
InP (buffer)	50	n	1 × 10^{18}
InP (contact)	800	n	1 × 10^{19}
InP	Substrate	-	-

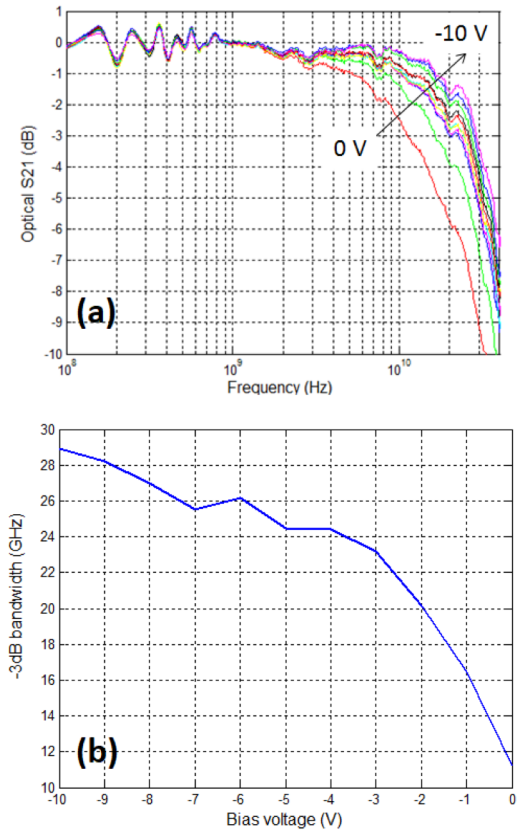

Fig. 4. *Calibrated RF responses* ***(a)*** *for the 5.5 µm × 25 µm long waveguide device for 0 to -10 V in steps of 1 V.* ***(b)*** *3-dB bandwidth plotted as a function of the device bias.*

calibrated using the VNA, a 40 GHz fiberized Mach-Zehnder modulator and a 65 GHz calibrated photodetector. The RF response was obtained under photocurrents of approximately 70 – 100 µA. The measurement results reveal a rapid increase of the bandwidth for reverse bias voltages down to -3 V; after this voltage the increase slows down. The experimental data show that the leakage current increases quite rapidly after -6 V. Therefore, the device bias voltage is kept at -5 V. The measured bandwidth for the 25 µm long PD is 25GHz at -5 V, while the longer 65 µm device has a considerably lower bandwidth of 11.5 GHz. This can be attributed to the *RC* time constant which acts as a limiting factor for the 3dB cut-off frequency. Increasing the PD length will decrease the active region resistance while the capacitance ($C_{eq}=\varepsilon A/d$) will be increased. For the intrinsic device it would not change the RC time constant. However, it should be noted that the n-contact of our device has not been changed while the ridge length has been increased. As a result, if the n-contact resistance is not small enough, the *RC* cut-off frequency will be decreased as measured in the experiment.

Simulations have been performed at a bias of -5 V, in line with the experimental results. At first, the theoretical models have been calibrated by modifying structural parameters, such as contact resistance, and using the proper physical models to reproduce the experimental results. We use here a 2D simulation framework, where the n-contact resistance is set to be 5 times smaller than the p-contact resistance, reflecting the wider n-contact of our grown UTC-PD. The

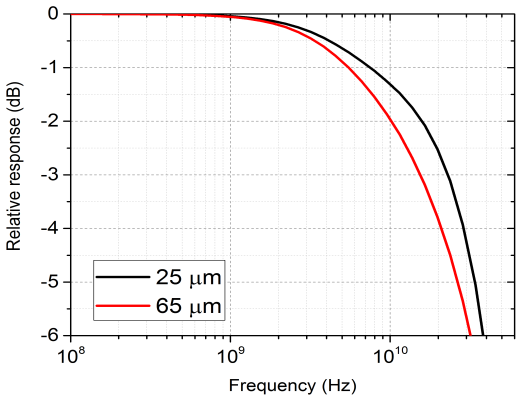

Fig. 5. *Simulated RF responses for the 25 µm and 65 µm long devices at a bias voltage of -5 V.*

structures investigated have a measured device resistivity of 10^{-4} Ω.cm^2, as determined by taking a dark-IV curve of the full device, measuring the slope resistance above turn-on, then dividing by the p-contact area. Since the contact resistance is smaller than that of the full device, we set the p-contact resistivity at 2×10^{-5} Ω.cm^2 and after calibration, the simulation results are in good agreement with the experimental data for both the 25 µm and the 65 µm device. The experimental 3-dB cut-off frequency measured for 25 µm and 65 µm devices are 25 and 11.5 GHz, respectively. The calibrated calculation gives 22 and 15 GHz for 25 µm and 65 µm, respectively. Simulated RF responses for the 25 µm and the 65 µm long device for -5 V are displayed in Fig. 5.

5. Results and discussions

The goal of this paper is to analyze the impact of changes in different parts of a UTC PD structure, including approaches which have been introduced in the literature to improve the performance of UTC PDs. We apply the changes to the UTC PD studied experimentally, in order to increase the 3-dB cut-off frequency of the UTC PD for faster optical communications. As noted earlier, the UTC structures investigated utilize depleted absorber [10] and cliff layers to enhance electron transport and reduce transit time. The cliff layer is used to elevate the electric field at the interface and to smooth the flow of carriers from the active region [12]. We also use barrier reduction layers [4] designed to smooth the flow of carriers across heterojunctions. In the following section, we present simulation results obtained by modifying different structural parameters. Here, we focus on the contact resistance (section 5A), cladding (section 5B), absorber (section 5C), collector and cliff layers (section 5D). Thickness and doping concentrations are changed and their impact on f_{3dB} is studied. In section 5.5 we then present the design of an optimized UTC PD and compare its photoresponse with that of the experimentally studied UTC PD.

5.1. Contact resistance

The results presented in Fig. 6 show that the impact of the contact resistance on the 3-dB cut-off frequency is very large. As noted earlier, the n-contact resistance is much smaller than the p-contact resistance. This stems from the much wider contact surface area. It can be seen that, by decreasing the contact resistance from 2×10^{-5}

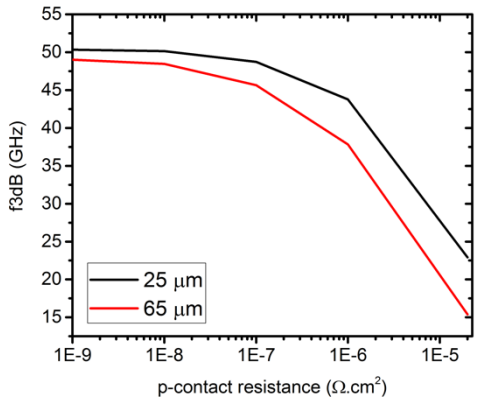

Fig. 6. *Effect of contact resistance on the 3dB cut-off frequency of UTC PD.*

$\Omega.cm^2$ to 1×10^{-7} $\Omega.cm^2$, an increase in the bandwidth of up to about 2-3 times can be achieved for the 25 µm and the 65 µm UTC PDs, respectively. Decreasing the contact resistance will decrease the *RC* time constant, which is a limiting factor for f_{3dB} in a PD. A smaller *RC* time constant enables a higher speed and f_{3dB}. This emphasizes the importance of minimising the contact resistance during the fabrication process of UTC PDs.

5.2. Cladding layer

The cladding layer is used to create an optical waveguide. The thickness of the cladding layer can affect the bandwidth. The effect of cladding layer thickness on the UTC PD bandwidth is displayed in Fig. 7, assuming a p-contact resistance of 1×10^{-6} $\Omega.cm^2$. It can be seen that a small reduction in the thickness of the cladding layer slightly increases f_{3dB}, which originates from decreasing the resistance imposed by this layer. It is worth noting that if the cladding layer is too thin, leakage of light up to the contact can be an issue for the edge-coupled WG UTC PD, which relies on the cladding for its optical waveguide. However, cladding layers as thin as 100 nm for UTC PDs incorporating thicker absorber layers can be found in the literature [17]. By removing the cladding layer entirely, a significant increase in the UTC PD bandwidth can be achieved. This, however, requires a wider redesign of the UTC PD, as a conventional edge-coupling scheme can no longer be used for light absorption. An evanescently coupled waveguide UTC PD [18] which was reported in the literature is one of these designs. However, in this paper our goal is to study edge-coupled WG UTC PDs. Therefore, we choose a cladding layer thickness of 600 nm,

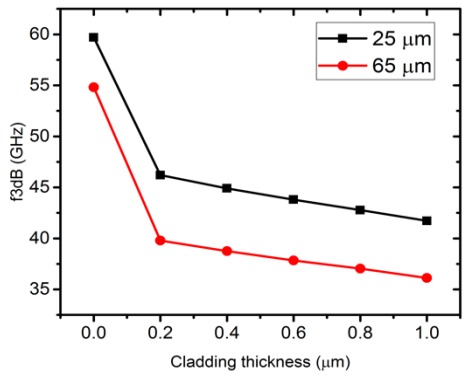

Fig. 7. *Effect of cladding layer thickness on the 3dB cut-off frequency of UTC PD.*

given that at this value f_{3dB} is not very different from the value at 200 nm (difference of approximately 5 GHz) and that leakage of the light up to contact is expected to be insignificant for a 600 nm cladding. Besides varying the cladding layer width, a slight increase of doping concentration in the cladding layer could also increase the bandwidth by decreasing the resistance. However, it should be noted that over saturation might increase the resistance at higher temperatures due to increased scattering from the dopant atoms.

5.3. Absorber layer

The influence of the absorber thickness and its doping concentration is depicted in Fig. 8 (a) and 8 (b), respectively. As shown in Fig. 8, decreasing the absorber layer thickness will lead to a higher 3-dB cut-off frequency. Increasing the absorber layer thickness increases the carrier traveling time and as a result decreases the speed and the f_{3dB} of the PD (Fig. 8 (a)). It should be noted that the self-induced field, which has its origin in the drift current of majority carriers (holes) in the absorber layer and which has been found to result in a significant increase in f_{3dB} [4], does not depend on the absorption layer thickness. However, the diffusive velocity drops with increasing absorption layer thickness. This problem can be reduced by allowing the doping concentration to vary with position in the absorption layer. Figure 8 (b) shows the calculated impact of the absorber layer doping concentration on the bandwidth of the UTC PD. It has been proposed [19], [20] that introducing step-like and gradient doping concentration profiles in the absorber layer lead to a speed up of electron diffusion towards the collector layer by forming a quasi-neutral electric field, which improves carrier transport [3]. Here we compare a constant doping concentration (1×10^{19} cm^{-3}) with graded doping concentrations in the absorber layer of the UTC PD. As can be seen in Fig. 8 (c), using a graded doping concentration can increase the average electric field in the absorption layer. This speeds up the carrier transport towards the depleted absorber layer and decreases the overall transit time, thereby increasing the bandwidth (cf. Fig. 8 (b)). The increase is more pronounced for thicker absorber layers. Further calculations that we carried out to vary the depleted layer thickness showed that f_{3dB} is almost independent of the thickness of the depleted layer for the range of values that we considered (0.04 to 0.10 µm). The depleted absorber layer is required to be undoped or to have a very low doping concentration. Given that any residual background doping may degrade the depletion effect in a wider depletion layer, we therefore choose to maintain a relatively narrow depletion layer of 0.05 µm in the optimized structure discussed below.

Overall, the highest f_{3dB} value in Fig. 8(a) is obtained for the thinnest absorber layer thickness, namely 0.05 µm, which we therefore choose as the optimum absorber layer thickness in Section 5.5. However, we note that using a Gaussian doping profile may allow a route to enhanced absorption efficiency, without degrading the overall bandwidth. Figure 8 (b) shows that the cut-off frequency is only slightly reduced for an absorber layer thickness of 0.11 µm, compared to that of the 0.05 µm system when using a Gaussian doping profile. Given that the absorption per unit length of the device scales approximately linearly with absorber layer thickness, it should therefore be possible to retain the same absorption efficiency in a shorter device by using a Gaussian doping profile and thicker absorber layer.

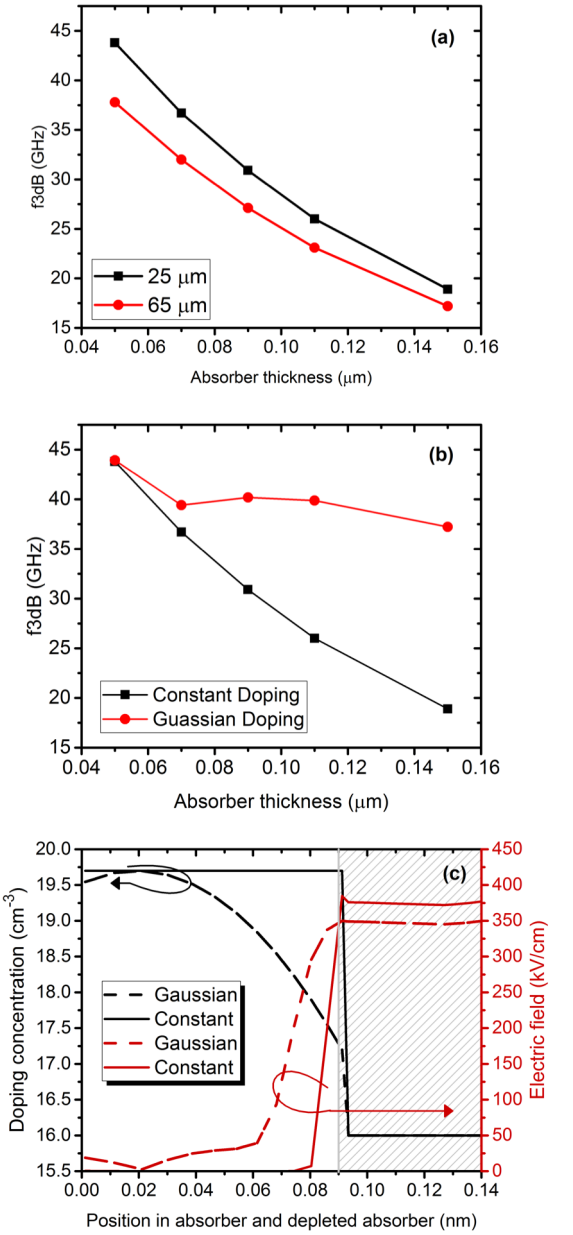

Fig. 8. *Effect of absorber layer* ***(a)*** *thickness and* ***(b)*** *doping concentration on the bandwidth of the UTC PD.* ***(c)*** *Gray markings represent the depleted absorber region. The electric fields and doping concentrations were extracted at a vertical cutline in the middle of the UTC PD.*

5.4 Collector and cliff layers

Figure 9 shows how the collector and the cliff layers can affect the bandwidth of the UTC PDs. We find here that thicker collector and cliff layers make the PD slower and lower the bandwidth. An increased resistance consequently increases the *RC* time constant and reduces the speed. A thicker collector layer means that the distance which photo-generated electrons have to travel to get to the n-type contact layer increases. As a result the transit time increases and the 3-dB cut-off frequency decreases. Therefore, based on studied thicknesses here and to achieve the highest f_{3db} values, the optimal thickness of the collector and cliff layer is 0.05 μm.

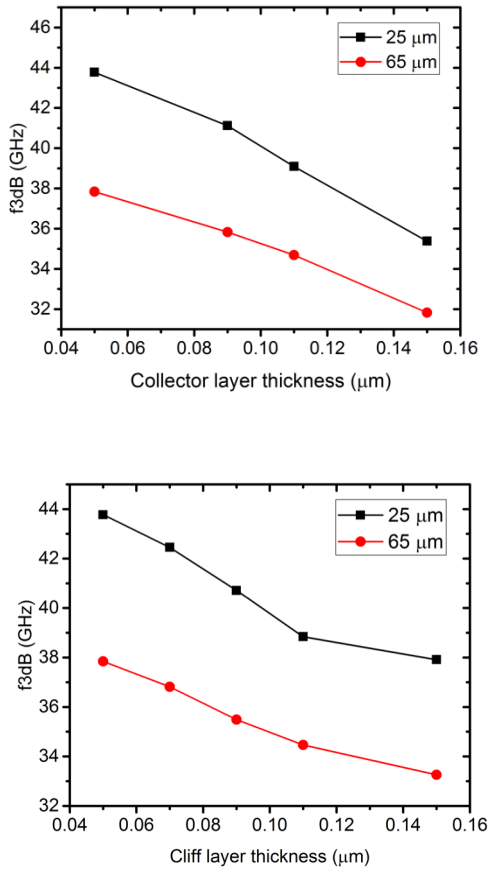

Fig. 9. *Effect of collector layer thickness (upper figure) and cliff layer thickness (lower figure) on the bandwidth of UTC PD.*

5.5 Optimized device

Now we collate our findings to design an improved UTC PD and compare its RF response with the RF response of the initial UTC PD. Building on our findings from above, we propose that the most critical step is to reduce the contact resistance. We assume in the device design that the p-doping resistance can be significantly reduced and we also apply a graded doping concentration in the absorber layer. Using a thin absorber layer decreases the electron transit time and an optimized cliff layer thickness increases the electric field at the interface and decreases also the carrier transit time. The proposed UTC PD structural parameters, using the above extracted optimal thicknesses for cladding, absorber, collector layer thicknesses, are shown in Table 2. Experimental data suggest that achieving a p-contact resistivity of 10^{-7} Ω.cm^2 should be feasible by optimizing the deposition through surface de-oxidation, evaporation of Ti-Pt-Au and alloying the contact. The cut-off frequency of the theoretically optimized UTC PD (49 GHz) is then a factor of two larger than that of the experimentally measured UTC PD (25 GHz).

6. Conclusion

In this work we have studied the effect of structural properties on the 3dB cut-off frequency (f_{3dB}) of edge-coupled WG UTC PDs. The UTC PD structure and contact resistances are important limiting factors of the bandwidth. Our goal was to increase the

Table 2 Structural parameters of the new UTC photodiode.

Material	Thickness (nm)	Type	Doping (cm^{-3})
InGaAs (contact+)	60	p	$>3 \times 10^{19}$
InGaAs (contact)	40	p	1×10^{19}
InGaAsP (barrier reduction)	20	p	2×10^{18}
InP (cladding)	600	p	2×10^{18}
InGaAsP (barrier reduction)	20	p	2×10^{18}
InGaAs (absorber)	50	p	Gaussian Doping* Peak at top: 1×10^{19}
InGaAs (depleted absorber)	50	n	$1\text{-}2 \times 10^{16}$
InGaAsP (barrier reduction)	20	n	2×10^{16}
InP (cliff)	50	n	2×10^{17}
InP (collector)	50	n	2×10^{16}
InP (buffer)	50	n	1×10^{18}
InP (contact)	800	n	1×10^{19}
InP	Substrate	-	-

*doping concentration decreases according to a Gaussian distribution with a standard deviation of 0.03 mm.

speed and cut-off frequency of the UTC PD by optimizing the different parts of such a device. Our investigation shows that the effect of the contact resistance on f_{3dB} is very large and that decreasing the contact resistance can increase the bandwidth significantly. This highlights the importance of reducing the contact resistance during the fabrication process of UTC PDs. We have also shown that (i) UTC PDs with decreased cladding layer thickness can show increased bandwidth, (ii) increasing the absorber layer thickness increases the carrier transit time and eventually decreases the 3dB cut-off frequency, (iii) using a graded doping concentration profile in the absorber layer can increase the cut-off frequency by increasing the average electric field in this region, with the bandwidth improvement being more pronounced for thicker absorber layers, and (iv) increasing the thickness of the cliff and collector layers will decrease f_{3dB} due to an increased resistance and an increased distance for electrons to travel into the n-type contact layer (which increases the transit time). Finally adopting all these findings, an optimized UTC PD is designed which should exhibit a significant increase in the 3dB cut-off frequency when compared to the initial structure investigated experimentally. More specifically, the new predicted UTC PD is expected to have a cut-off frequency of 49 GHz, which is much larger than the value of 22 GHz that we obtain theoretically for the experimentally realized structure.

7. Acknowledgments

We thank Science Foundation Ireland for funding this work as an IPIC Platform research project (12/RC/2276). The authors thank Matthew Smith, James O'Callaghan and Agnieszka Gocalinska for their contributions in device fabrication and materials growth.

8. References

[1] Tavernier, F., and Steyaert, M., *High-speed optical receivers with integrated photodiode in nanoscale CMOS*. Springer Science & Business Media, 2011.

[2] Ishibashi, T., Kodama, S., Shimizu, N., and Furuta, T., "High-speed response of uni-traveling-carrier photodiodes," *Jpn. J. Appl. Phys.*, vol. 36, no. 10R, p. 6263, 1997.

[3] Meng, Q., Wang, H., Liu, C. *et al.*, "High-Speed and High-Responsivity InP-Based Uni-Traveling-Carrier Photodiodes," *IEEE J. Electron Devices Soc.*, vol. 5, no. 1, pp. 40–44, 2017.

[4] Ishibashi, T., Furuta, T., Fushimi, H. *et al.*, "InP/InGaAs uni-traveling-carrier photodiodes," *IEICE Trans. Electron.*, vol. 83, no. 6, pp. 938–949, 2000.

[5] Klamkin, J., Ramaswamy, A., Chang, Y.-C. *et al.*, "Uni-traveling-carrier photodiodes with increased output response and low intermodulation distortion," in *Microwave Photonics, 2007 IEEE International Topical Meeting on*, 2007, pp. 14–17.

[6] Muramoto, Y., Fukano, H., and Furuta, T., "A polarization-independent refracting-facet uni-traveling-carrier photodiode with high efficiency and large bandwidth," *J. Light. Technol.*, vol. 24, no. 10, pp. 3830–3834, 2006.

[7] Guo, L., Huang, Y., Duan, X. *et al.*, "High-speed modif ied uni-traveling-carrier photodiode with a new absorber design," *Chinese Opt. Lett.*, vol. 10, no. s1, p. S12301, 2012.

[8] Srivastava, S., "Simulation study of InP-based uni-traveling carrier photodiode," University of Cincinnati, 2003.

[9] Zhou, Q., Cross, A. S., Beling, A. *et al.*, "High-power V-band InGaAs/InP photodiodes," *IEEE Photon. Technol. Lett.*, vol. 25, no. 10, pp. 907–909, 2013.

[10] Jun, D.-H., Jang, J.-H., Adesida, I., and Song., J.-I., "Improved efficiency-bandwidth product of modified uni-traveling carrier photodiode structures using an undoped photo-absorption layer," *Jpn. J. Appl. Phys.*, vol. 45, no. 4S, p. 3475, 2006.

[11] Shimizu, N., Watanabe, N., Furuta, T., Ishibashi, T., "InP-InGaAs uni-traveling-carrier photodiode with improved 3-dB bandwidth of over 150 GHz," *IEEE Photonics Technol. Lett.*, vol. 10, no. 3, pp. 412–414, 1998.

[12] Li, Z., Pan, H., Chen, H., Beling, A., and Campbell, J. C., "High-saturation-current modified uni-traveling-carrier photodiode with cliff layer," *IEEE J. Quantum Electron.*, vol. 46, no. 5, pp. 626–632, 2010.

[13] Jin, L., Xiong, B., Luo Y. *et al.*, "Ultrafast dual-drifting layer uni-traveling carrier photodiode with high saturation current," *Opt. Express*, vol. 24, no. 8, pp. 8420–8428, 2016.

[14] Banik, B., Vukusic, J., Hjelmgren, H. *et al.*, "UTC-PD Integration for Submillimetre-wave Generation," in *19th International Symposium on Space Terahertz Technology*, 2008, p. 7.

[15] SILVACO, Inc., "ATLAS User's Manual," *Santa Clara, CA,* 2016.

[16] Sharma, R., K., Gupta, R., Gupta, M., and Gupta, R. S., "Dual-material double-gate SOI n-MOSFET: gate misalignment analysis," *IEEE Trans. Electron Devices*, vol. 56, no. 6, pp. 1284–1291, 2009.

[17] Beling, A., Xie, X. and Campbell, J. C., "High-power, high-linearity photodiodes," *Optica*, vol. 3, no. 3, pp. 328–338, 2016.

[18] Sun, S., Liang, S., Xu, J. *et al.*, "Evanescently Coupled Waveguide InGaAs UTC-PD Having an Over 21 GHz Bandwidth Under Zero Bias," *IEEE Photonics Technol. Lett.*, vol. 29, no. 14, pp. 1155–1158, 2017.

[19] Li, C., Xue, C.-L., Li, C.-B. *et al.*, "High bandwidth surface-illuminated InGaAs/InP uni-travelling-carrier photodetector," *Chinese Phys. B*, vol. 22, no. 11, p. 118503, 2013.

[20] Li, C., Xue, C.L., Liu, Z. *et al.*, "High-responsivity vertical-illumination Si/Ge uni-traveling-carrier photodiodes based on silicon-on-insulator substrate," *Sci. Rep.*, vol. 6, p. 27743, 2016.